

Chapter 5

Lensless Fourier Transform Digital Holography for microscopy and mapping Spatio-temporal evolution of refractive index for defect detection

5.1 Lensless Fourier Transform Digital Holography

This chapter describes the utilization of speckle field with the digital holography technique (1) to study Spatio-temporal evolution of refractive index in a dielectric slab and use this information for defect detection (2) quantitative phase contrast imaging of micro-objects such as human erythrocytes also known as Red Blood Cells (RBCs).

Since its conception, Digital holography has emerged as one of the most sought-after techniques for recording and reconstruction of the 3D field. It has been extensively used for a variety of industrial and biomedical applications where it is employed especially for metrological and imaging purposes [239–251]. The development of high-quality detectors and processing algorithms for digital reconstruction of the hologram has revolutionized the technique of Digital holography [252–255]. It is an imaging technique that yields the complex amplitude of the object wavefront by numerically reconstructing the digitally recorded holograms using scalar diffraction theory. The phase of the object wavefront can be deduced from the numerically reconstructed complex amplitude distribution [253,256,257]. The phase information together with the amplitude provides quantitative data about the object. The ability of numerical focusing allows the measurement of the complex amplitude across any plane parallel to the recording plane using diffraction integral [256]. Advantages such as numerical focusing, single-shot imaging capability, have earned digital holography a very important place in the field of imaging and metrology [258,259]. And thus, it finds immense potential in applications ranging from shape measurement to microscopy [253,256,257,260–287].

Digital holography is especially useful in the case of phase objects, which do not produce a significant change in the amplitude of the interacting wavefront and hence are difficult to image [260–279,281,283,286,287]. Since they introduce a

change in the optical path length, the phase of the wavefront changes, which can be helpful in imaging, quantifying and characterizing phase objects [269–279,281]. Since most of the biological cells are transparent to visible radiation, Digital Holography can be very useful in studying/imaging such as microscopic objects. The Off-axis Digital Holographic microscopy is a single-shot technique to reveal the phase information, and is an ideal tool to investigate the dynamics of micro-objects including cells from a series of recorded holograms/ interferograms [261,262,270,273,283,288–296]. The main disadvantage of DH microscopy employing a two-beam configuration is that it is more prone to mechanical vibrations. Since the two beams travel along different paths, they can acquire phase changes (due to vibration), which are uncorrelated, leading to low temporal stabilities [297]. This affects the measurement of dynamic events like cell membrane fluctuations. To overcome this hurdle one would like to have a single path and single-shot setup providing direct access to phase information [297–304]. Techniques which convert the object beam into two beams provide such an option. Object information is removed from one of the beams by means of filtering and this beam acts as the reference beam [298,299]. Self-referencing techniques can also be used to improve the stability of the system. In this class of interferometers, a part of the object beam that does not exhibit sample structure acts as the reference beam [297,300–304]. The biggest advantage of the self-referencing techniques is that no special optical element is required to convert the object beam into a reference beam. However, this method has the disadvantage that only a portion of the field of view will be useful. This can be overcome by the use of a pinhole in the path of the object beam leading to a lensless Fourier transform digital holography (LFTDH) setup, where the reference beam originates from a point source located at the plane of the object [255,272]. The configuration of the lensless Fourier transform digital holography (LFTDH) generally requires a lens but not a Fourier transforming lens [182]. It was first invented by G. W. Stroke in 1965 [305]. The Fourier transform is optically implemented by employing a lens, where the transformation is carried out between the complex amplitude distribution of the object field in the pupil and the complex amplitude distribution of the object field in the focal plane of the

focusing system. However, this optical arrangement is devoid of the advantages of lensless holographic imaging [305,306]. Therefore, to avail the advantages of lensless imaging together with the benefits of digital holography, the concept of Lensless Fourier transform Digital Holography (LFTDH) was developed and applied [305]. The reference beam is made up of a spherical wavefront that has its origin at the reconstruction plane and in most applications located at the object plane. Hence, the position and characteristics of the reference beam depend on the position of the object with respect to the recording modality [252,255,305,307].

Some of the numerical reconstruction algorithms such as the Fresnel approach and the Convolution approach involve several fast Fourier transforms and require performing complex computation [255]. The configuration of the LFTDH technique gives an edge over other methods because of its simplistic approach towards the numerical reconstruction of the holograms[308]. The LFTDH technique requires only a single Fourier transform and achieves high lateral resolution. The LFTDH configuration allows the utilization of larger spatial bandwidth of the digital sensor. The LFTDH has two main advantages which include efficiently using the bandwidth of CCD in the recording process thereby improving the resolution of the reconstructed image, determining the position of the reconstructed image becomes independent of the recording distance and only depends on the distance between the object and the coplanar reference point source, and use of a single Fourier transform for obtaining complex amplitude.

Rayleigh's integral formula towards the scalar diffraction integral is one of the most accurate approaches for optical wave field propagation [309]. But the most general case is of the Fresnel approach and the Fresnel holograms are the most generated in holographic interferometry [151]. According to the Fresnel diffraction, the process of propagation can be expressed in terms of a single Fourier transform [182].

The Fresnel-Kirchhoff integral which describes the diffraction of a light wave at an aperture (hologram) placed perpendicular to the incident beams is expressed as

$$\Gamma(\xi, \eta) = \frac{i}{\lambda} \int_{-\infty}^{\infty} \int_{-\infty}^{\infty} h(x, y) R(x, y) \frac{\exp\left(-i \frac{2\pi}{\lambda} \rho\right)}{\rho} \left(\frac{1}{2} + \frac{1}{2} \cos \theta\right) dx dy \quad (5.1)$$

where
$$\rho = \sqrt{(x - \xi)^2 + (y - \eta)^2 + d^2} \quad (5.2)$$

(x, y) is the hologram plane, the (ξ, η) is the image plane, $h(x, y)$ is the hologram function, ρ is the distance between a point in the hologram plane and a point in the reconstruction plane, and θ is the angle between ρ and the perpendicular line joining the (x, y) and (ξ, η) planes [253] as shown in the Fig. 5.1.

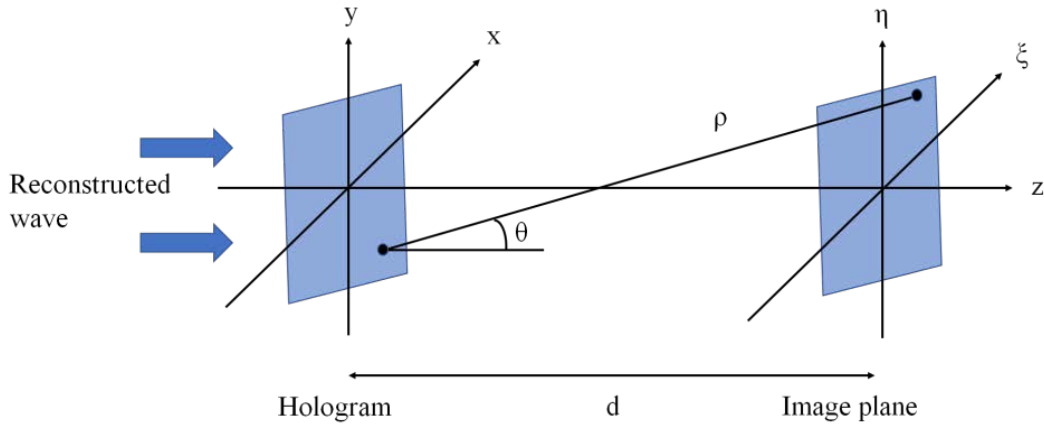


Fig 5. 1: Coordinate system for the numerical reconstruction process

The complex amplitude is calculated in the plane of real image and thus d is the distance behind the CCD plane at which the diffraction pattern is calculated. By applying the Fresnel approach and considering the values of x, y, ξ , and η to be small compared to the distance d , the first term of the Taylor series expansion of Eq. (5.2) is given by

$$\rho = d + \frac{(\xi - x)^2}{2d} + \frac{(\eta - y)^2}{2d} - \frac{1}{8} \frac{[(\xi - x)^2 + (\eta - y)^2]^2}{d^3} + \dots \quad (5.3)$$

$$\approx d + \frac{(\xi - x)^2}{2d} + \frac{(\eta - y)^2}{2d} \quad (5.4)$$

It is assumed that the angle θ is very small and thus $\cos \theta \approx 1$. Substituting the value of d obtained from Eq.(5.4) in Eq. (5.1):

$$\Gamma(\xi, \eta) = \frac{i}{\lambda d} \exp\left(-i \frac{2\pi}{\lambda} \rho\right) \int_{-\infty}^{\infty} \int_{-\infty}^{\infty} R(x, y) h(x, y) \times \exp\left[-i \frac{\pi}{\lambda d} ((\xi - x)^2 + (\eta - y)^2)\right] dx dy \quad (5.5)$$

Eq. (5.5) is further simplified to obtain

$$\Gamma(\xi, \eta) = \frac{i}{\lambda d} \exp\left(-i \frac{2\pi}{\lambda} \rho\right) \exp\left[-i \frac{\pi}{\lambda d} (\xi^2 + \eta^2)\right] \int_{-\infty}^{\infty} \int_{-\infty}^{\infty} R(x, y) h(x, y) \times \exp\left[-i \frac{\pi}{\lambda d} (x^2 + y^2)\right] \exp\left[-i \frac{2\pi}{\lambda d} (x\xi + y\eta)\right] dx dy \quad (5.6)$$

Eq. (5.6) is referred as the Fresnel approximation or Fresnel transformation and it provides the complex amplitude of the wavefield in the image plane. The complex amplitude at the virtual plane can be obtained by considering the image properties of the lens (Focal length $f = d/2$ to get a magnification of 1) into the numerical reconstruction process. The complex amplitude in the image plane is then calculated by

$$\Gamma(\xi, \eta) = \frac{i}{\lambda d} \exp\left(-i \frac{2\pi}{\lambda} \rho\right) \exp\left[-i \frac{\pi}{\lambda d} (\xi^2 + \eta^2)\right] \int_{-\infty}^{\infty} \int_{-\infty}^{\infty} R(x, y) L(x, y) h(x, y) \times \exp\left[-i \frac{\pi}{\lambda d} (x^2 + y^2)\right] \exp\left[-i \frac{2\pi}{\lambda d} (x\xi + y\eta)\right] dx dy \quad (5.7)$$

Rearranging Eq. (5.7)

$$\Gamma(\xi, \eta) = \frac{i}{\lambda d} \exp\left(-i \frac{2\pi}{\lambda} \rho\right) \exp\left[-i \frac{\pi}{\lambda d} (\xi^2 + \eta^2)\right] \int_{-\infty}^{\infty} \int_{-\infty}^{\infty} R(x, y) h(x, y) \times \exp\left[+i \frac{\pi}{\lambda d} (x^2 + y^2)\right] \exp\left[i \frac{2\pi}{\lambda d} (x\xi + y\eta)\right] dx dy \quad (5.8)$$

According to the description of LFTDH, the reference wave is a spherical wave whose source is located at the object plane and is given by

$$R = \frac{\exp\left(-i \frac{2\pi}{\lambda} \sqrt{(d^2 + x^2 + y^2)}\right)}{\sqrt{(d^2 + x^2 + y^2)}} \quad (5.9)$$

$$\approx \frac{1}{d} \exp\left(-i \frac{2\pi}{\lambda} \rho\right) \exp\left(-i \frac{\pi}{\lambda d} (x^2 + y^2)\right) \quad (5.10)$$

Substituting Eq. (5.10) in reconstruction formula for the virtual image Eq. (5.8) leads to:

$$\Gamma(\xi, \eta) = C \exp\left[-i \frac{\pi}{\lambda d} (\xi^2 + \eta^2)\right] \mathfrak{F}^{-1}\{h(x, y)\} \quad (5.11)$$

where C is a complex constant. It can be inferred from Eq. (5.11) that a single Fourier transform can reconstruct the lensless Fourier hologram. Hence, the use of a spherical reference wave generated at the object plane in this LFTDH configuration eliminates the effect of the spherical phase factor associated with the Fourier transform [253] and thus a single Fourier Transform can provide the complex amplitude of the object wavefront.

These aforementioned applications employ a single beam setup for LFTDH that provides a compact configuration [264,310] having lesser components in comparison to the conventional two beam setups while the use of speckle field helps in increasing the field of view by allowing the information from larger area of the object to be collected at the recording medium [50].

5.2 Spatio-temporal evaluation of refractive index in Dielectric materials

5.2.1 Introduction

An industrial product must fulfill certain parameters based on its utility as the consumers these days have a high level of expectations. It should perform as per the assigned function and give trouble-free service for a reasonable period. This has led companies to constantly increase the quality of their products. By improving its quality, the reliability and the safety can be enhanced which helps in increasing the production and reducing the scrap levels leading to good economic returns. This gave rise to the need for characterizing the products, locating and measuring

defects, which brought with it many new challenges of developing reliable advanced measurement and testing methods. Generally, measurement methods are categorized into two types (i) non-destructive and (ii) conventional contact methods. Depending upon the object and its dimension both these types have their own advantages and disadvantages [311]. The requirement for noncontact evaluation of the properties of a material, component or system has led to the development of the whole new branch known as Non-Destructive Testing (NDT), which is based on the principle of defect detection without affecting the function of the object under study [312–314]. NDT plays an important role in quality control in the case of finished items as well as raw materials. The method to be used depends on many factors such as dimension, location, state and material of the sample under observation. As optical techniques provide non-contact and non-destructive ways of imaging and measuring physical quantities with high precision, accuracy and sensitivity, they are being used extensively these days [312–314]. In addition to these qualities, the optical techniques are immune to electromagnetic interference and have the advantage of signal multiplexing.

Spatial variation in the phase of the wavefront is observed due to the refractive index distributions existing inside phase objects such as gaseous systems, temperature distributions produced by flames, plasmas, objects under thermal stress, biological specimens, etc [151,239,315]. The refractive index, in turn, depends upon many parameters such as density, temperature, impurity distribution, etc. Thus, by mapping the refractive index across the object which is subjected to thermal stress, the thermal conductivity of objects can be studied. And by taking into account the fact that regions with different refractive indices will have different thermal conductivity, optical inhomogeneities can be imaged as a discontinuity in the refractive index distributions leading to defect detection in transparent as well as in translucent objects. Various optical techniques like the Shadow, Schlieren and interferometric techniques, can be used to map the refractive index profile of phase objects [151,239,315–323]. These methods yield the second derivative of the refractive index profile, the derivative of the refractive index and the refractive index respectively. So, the interferometric methods have an advantage over the

other two even though it must satisfy stringent optical conditions. Also, a change in temperature in the case of fluids and solids leads to a change in their refractive index profile and this change can be imaged as a phase variation using digital holography, which in turn can be used for characterizing the sample under investigation [273]. Lens-less Fourier transform digital holography geometry uses a point reference located exactly at the object plane [253,256,264,272], which enables numerical reconstructions employing a single Fourier transform, leading to real-time monitoring of object phase changes. Here we describe our efforts in the development of a single beam wavefront division lens-less Fourier transform digital holographic interferometric technique for imaging of spatio-temporally evolving refractive index distributions and using the same for defect detection in case of transparent and semitransparent objects subjected to thermal stressing.

5.2.2. Experimental realization

A simple single beam setup using a pin-hole co-located with the diffuser is devised to record lens-less Fourier transform digital holograms of phase objects for mapping their refractive index distributions leading to the determination of the defects in the investigated samples [264].

Fig. 5.2 shows the schematic of the devised setup. A He-Ne laser of wavelength 611.9 nm and having a maximum output power of 2mW is used as the source. The expanded and collimated output from the laser trans-illuminated the phase object under investigation and is converted into volume speckle field by a diffuser and acted as the object wavefront. The roughness of the diffuser is measured by using reflection mode digital holography [324] and is found to be 0.37 μm . In the setup shown in Fig. 5.2, to create the reference point source located at the diffuser plane, a pin-hole of an approximate diameter of 200 μm is made on the diffuser using a hot needle. This pin-hole samples a portion of the wavefront falling on the diffuser creating a wavefront division geometry. The object and reference wavefronts interfere at the detector plane to create the holograms (Fig. 5.3), which are recorded by a CCD array (8-bit dynamic range, 4.65 μm pixel pitch).

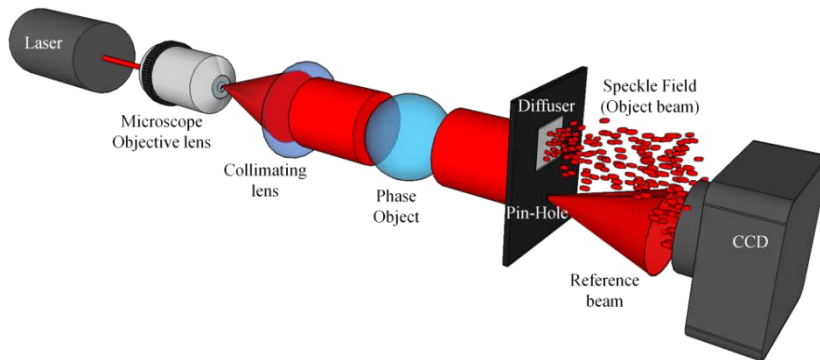


Fig 5. 2: Single beam lens-less Fourier transform holography setup for investigation of phase objects

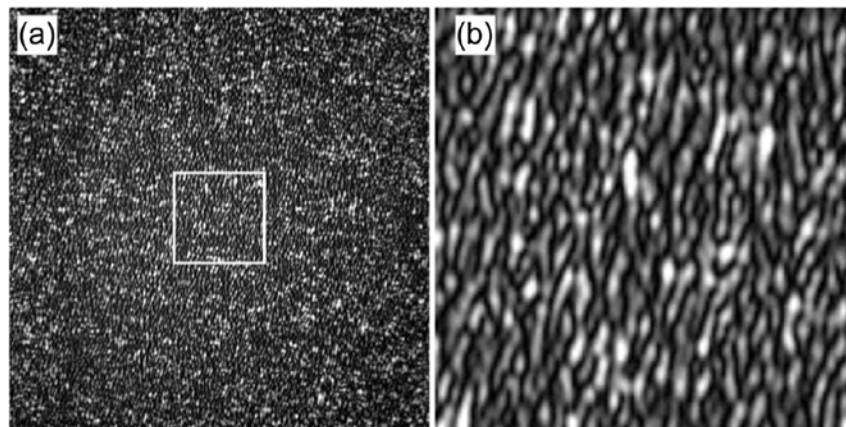


Fig 5. 3: (a) Hologram recorded using the setup in Fig. 1. (b) Area inside region of interest showing the holographic fringes

To investigate spatio-temporally evolving objects, a sequence of digital holograms are recorded. The numerical reconstruction of digital holograms is achieved by illuminating the hologram by a digital version of the reference wavefront [253]. Diffraction of the reference wavefront from the micro-structures of the hologram, which is kept perpendicular to the reference incoming beam, is described by the Fresnel-Kirchhoff integral after applying Fresnel approximation [182,253] according to Eq. (5.11).

So, a lens-less Fourier transform hologram is reconstructed by a single Fourier transform yielding the complex amplitude distribution (an array of complex numbers) of the entire object [253,256,264,272]. The intensity and the phase of the object wavefront can be determined from this complex amplitude [264,272]. The phase of the object wavefront at any time instance is computed from the complex amplitude using

$$\phi(x, y, t) = \tan^{-1} \left\{ \frac{\text{Im}[U(x, y)]}{\text{Re}[U(x, y)]} \right\} \quad (5.12)$$

where ‘Re’ and ‘Im’ represents the real and imaginary part of the reconstructed complex amplitude distribution. To study the time evolution of a phase object under stress, phase at two different time instances (t_1 and t_2) are compared. Digital holography provides an advantage of directly comparing the phase of the object wavefronts existing at two-time instances through

$$\begin{aligned} \Delta\phi(x, y) &= \phi(x, y, t_2) - \phi(x, y, t_1) \\ &= \frac{2\pi}{\lambda} [n(x, y, t_2) - n(x, y, t_1)] z \\ &= \frac{2\pi}{\lambda} \Delta n(x, y, t_2, t_1) z \end{aligned} \quad (5.13)$$

where the z is the length of the sample through which the probe beam passes, $n(t_2)$ and $n(t_1)$ are the refractive indices at two different time instances and Δn is the refractive index change between the two time instances. The phase difference attained by a ray propagating in the z direction is proportional to the refractive index change $\Delta n(x, y)$ according to

$$\Delta\phi(x, y) = \frac{2\pi}{\lambda} \int_{z_1}^{z_2} [n(x, y, z) - n_0] dz \quad (5.14)$$

where $n(x, y, z)$ is the position dependent refractive index inside the medium and n_0 is the constant average refractive index of the medium before perturbation.

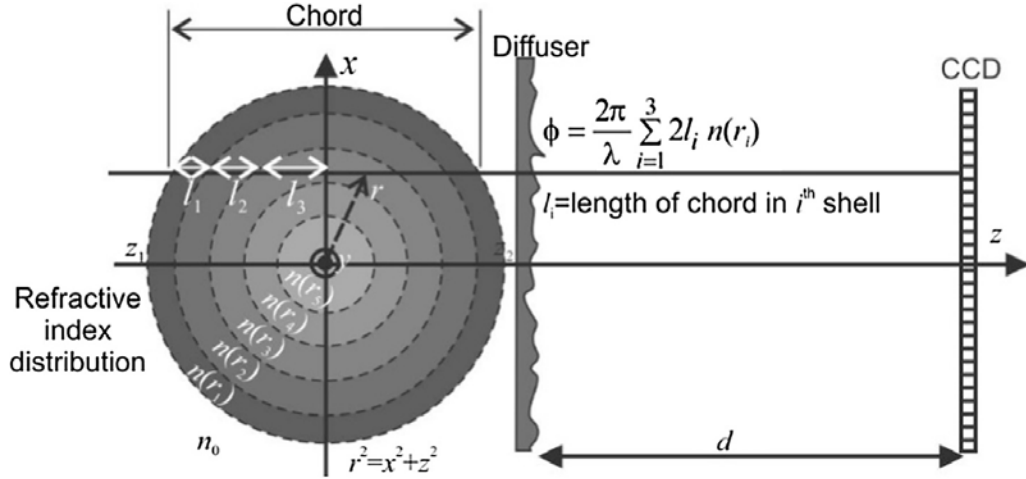


Fig 5. 4: Refractive index distribution inside axi-symmetric phase object. In axi-symmetric case, the refractive index depends only on the distance (r) from the axis of symmetry (in this case y -axis)

In the case shown in Fig. 5.4 (cross-section of a cylindrical object), the y -axis is the axis of symmetry and light propagates along the z -direction. So the refractive index varies in the x - z plane. For axisymmetrical phase objects, this refractive index distribution can be represented as a function of r ($r^2 = x^2 + z^2$) alone as shown in Fig. 5.4. It means that the refractive index values depend only upon the distance from the axis of symmetry. So, in the axisymmetric case, the refractive index can be assumed to be having constant values in concentric shells. Each ray of light (it is assumed that the ray is not refracted and picks up phase change due to optical path change only) passes through several shells and picks up refractive index information from all the shells it passes through. So phase change accrued by each ray is a sum of the optical path lengths (depending upon the chord length and local refractive index) picked up from different shells (Fig. 5.4). These are called as the chord integrated values and is represented by Eq. (5.14), which is the Abel integral equation [316]. Tomographic inversion of the chord integrated values is required to yield the local values of the refractive index $n(r)$. Several objects like flames, transparent dielectric slabs exposed to point heat source, plasmas (especially laser-produced), jets, etc have this type of refractive index distribution. In such objects, the local changes in phase can be computed by Abel inversion of the chord integrated phase values [316].

5.2.3. Phase imaging capability

Before applying the above-discussed technique for detecting defects, the phase imaging capability of the technique is evaluated. A candle flame is used as the object to map its refractive index profile. A reference hologram is recorded when the flame was unlit. After the candle is lit a series of object holograms at different stages of the flame are recorded.

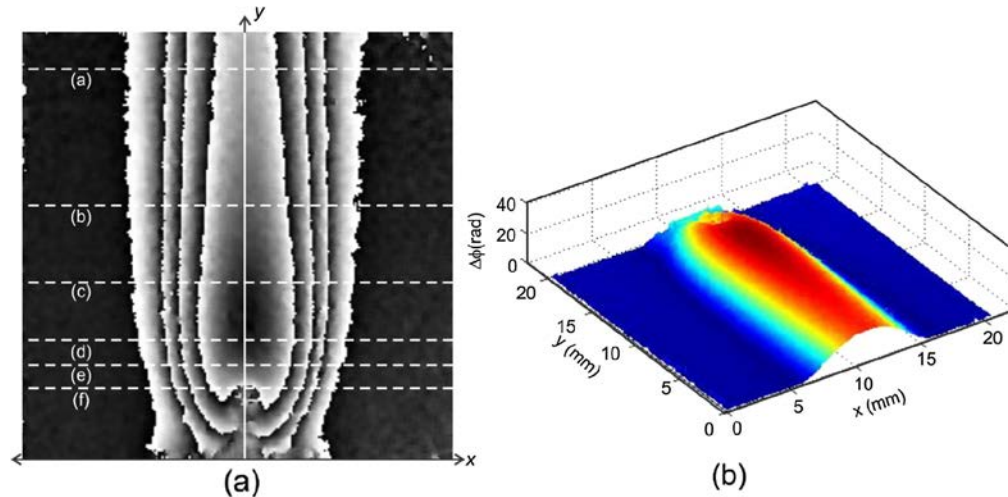


Fig 5. 5: Phase contrast images of the refractive index distribution (a) wrapped phase distribution and (b) three-dimensional representation of the phase distribution obtained after unwrapping. Chord integrated phase profiles along the lines in (a), were Abel inverted to obtain the local refractive index values (which varies radially)

Fig. 5.5 shows the phase difference profile in the case of the candle flame. Fig.5.5(a) represents the wrapped phase which is converted into continuous phase distribution using Goldstein's branch cut unwrapping algorithm (Fig. 5.4(b)). The phase distribution in the case of a candle flame is axisymmetric.

Fig. 5.6 shows the variation in chord integrated phase profile along the dashed lines (along the x-axis) shown in Fig. 5.5(a). Since the phase profile is axisymmetric, from one phase profile, using Abel inversion, local refractive index changes can be determined [316].

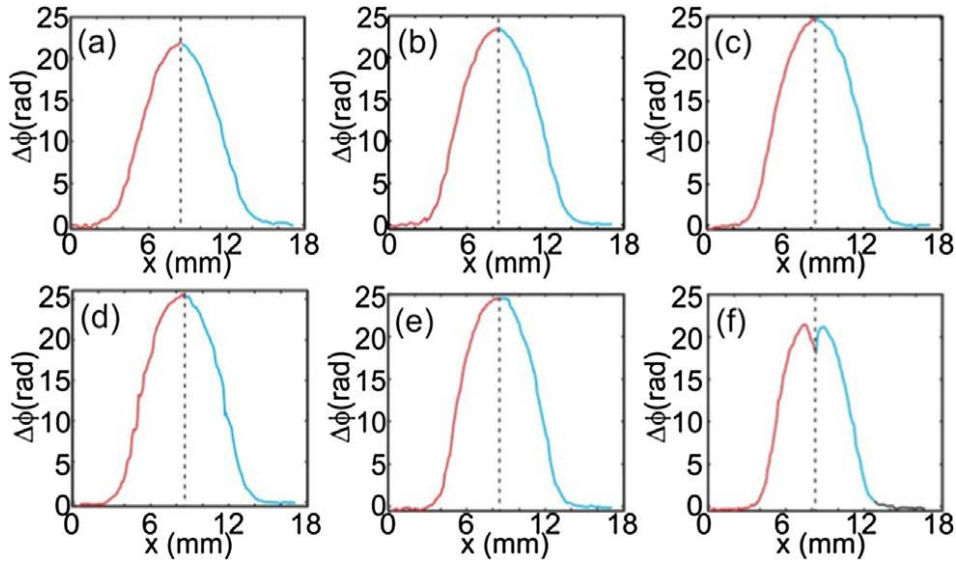


Fig 5. 6: Chord integrated phase profiles obtained from the reconstructed holograms at different positions in the flame. Left and right side of the distribution are color coded in red and blue respectively. They are individually used in Abel integral to obtain the refractive index distributions.

Fig. 5.7 shows the local change (radial) in the refractive index for the chord integrated data shown in Fig. 5.6. Chord integrated data on the right side of the distribution is used to obtain local refractive index changes on the right of the Abel inverted profile and similarly for chord integrated data on the left side is used to obtain Abel inverted profile on the left side. The difference in temperature across the candle is reflected as the variation of the refractive index. As the refractive index is mapped, it is seen from Fig. 5.5(b) that the candle has a higher change in temperature at the centre, and the temperature change decreases at the outer regions. Also, near the wick of the candle refractive index change is small indicating less change in temperature which is as expected.

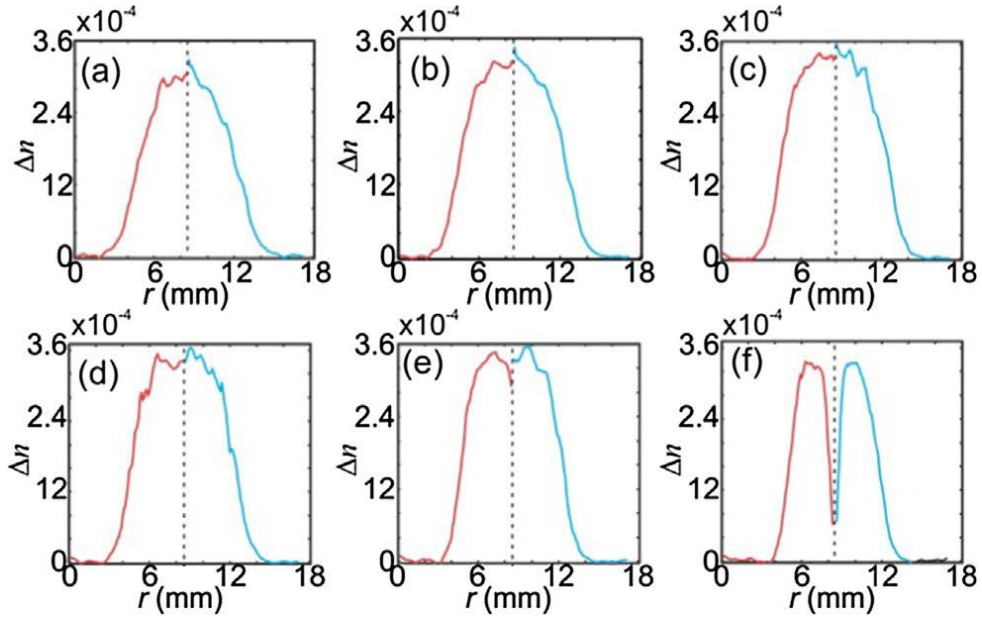


Fig 5. 7: Radial distribution of refractive index inside the flame obtained after Abel inversion of the chord integrated data shown in Fig. 5.6a–f

5.2.4. Dynamic phase imaging

Before applying the developed technique on time-evolving phase distributions, its temporal stability is measured by recording a sequence of holograms (recorded for 10 min at the rate of 20 Hz) using only the diffuser without introducing a phase object. The phase is reconstructed from each of the recorded holograms. The mean (across the field of view) of the standard deviation of phase variation (thickness fluctuation) with time acts as the measure of the temporal stability of the technique [266]. Fig. 5.8 shows the histogram of the thickness fluctuation over the imaged field of view. The mean value of these fluctuations is 6.16 nm over a 10 min period and this value acts as the temporal stability of the system. It should be noted that the technique is implemented without any vibration isolation mechanism.

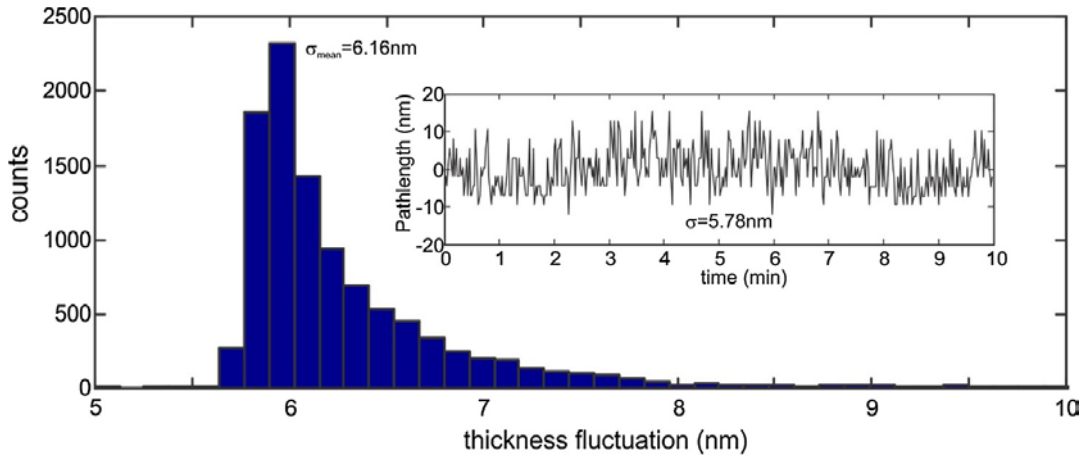


Fig 5. 8: Histogram of path length fluctuation across the field of view. Inset shows the pathlength variation as a function of time

The developed technique is used to image and study heat transfer in translucent materials. A fused silica glass plate of dimension 50mm×50mm×24 mm, where 24 mm represents the thickness of the glass plate. It is placed behind the ground glass diffuser and was heated continuously by the tip of a heating rod kept 5mm from the plate. The heating rod can be considered as a point source. The phase is calculated over the time interval by subtracting the phase obtained for the object at room temperature. Fig. 5.9 shows the spatio-temporal phase evolution for the heated glass plate.

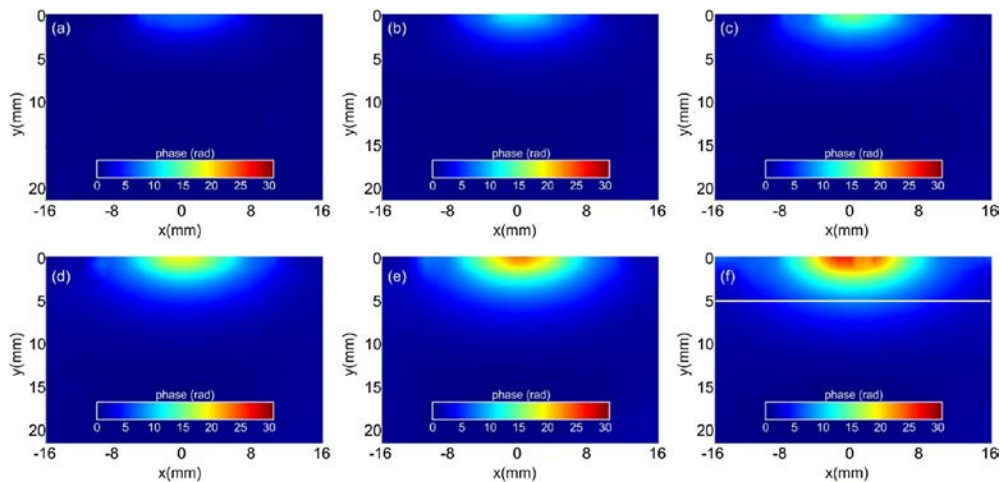


Fig 5. 9: (a)–(f) Spatiotemporal evolution of phase difference for a fused silica glass slab exposed to a heating rod. Each frame is separated in time by 10 s

It can be seen that the phase distribution is axisymmetric. The axis of symmetry is located at $x=0\text{mm}$ and the phase variation along the x -direction at any y -position can be Abel inverted to obtain the local change in refractive index. Fig. 5.10(a) shows the chord integrated value along the line shown in Fig. 5.9(f). Local refractive index changes obtained after Abel inversion is shown in Fig. 5.10(b). Here also the local values for the left and right side are computed using chord integrated values on the left and right side respectively.

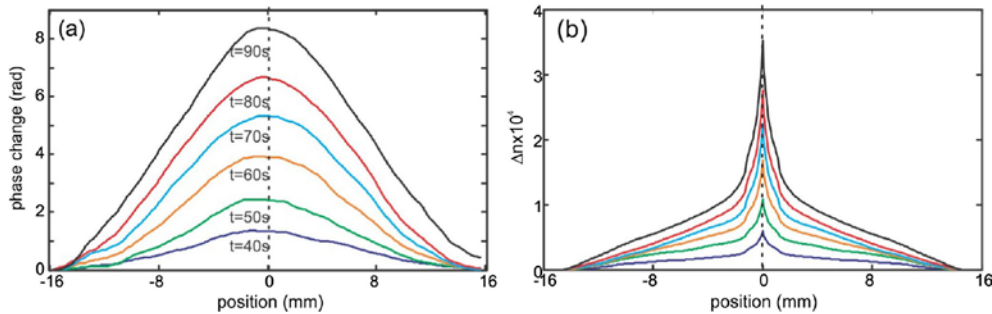


Fig 5. 10: (a) Chord integrated phase values along the line shown in Fig. 8f. (b) Local values of refractive index change obtained after Abel inversion

5.2.5 Defect detection by thermal stressing

From Fig. 5.9 it can be seen that as the heat diffuses uniformly into the sample, its refractive index distribution changes. If there is any discontinuity (defect) in the medium, the heat flow across the discontinuity will be different, since its thermal conductivity will be different, from that of the medium surrounding the discontinuity. This will result in a different phase distribution across the discontinuity. The developed technique can be used to measure this change in phase across the defect to image, quantify and characterize it. The technique is applied on a plexiglass sheet of 1 cm thickness on which a hole is made using a heated pin. This object is kept behind the ground glass diffuser and holograms were recorded at the rate of 1 every 10 s for 5 min as the sample is heated (Fig. 5.11).

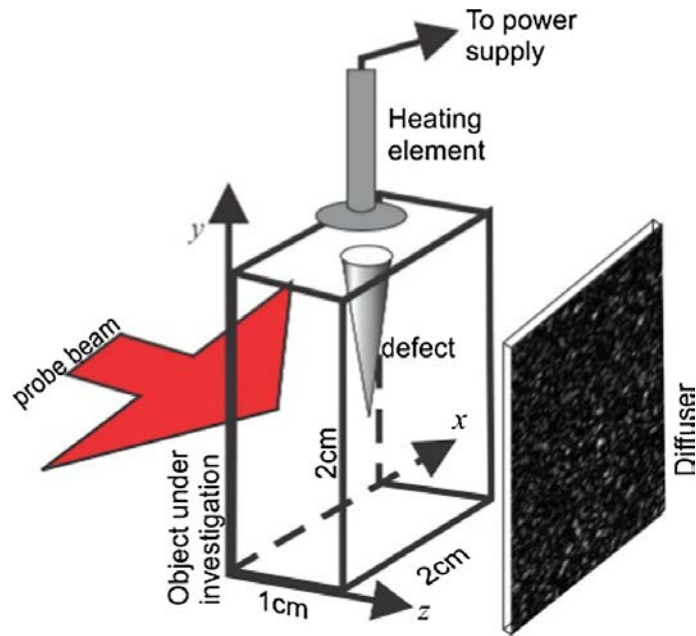


Fig 5. 11: Thermal stressing of the sample using a heating rod

Phase difference for each time instance is computed by subtracting the phase obtained at $t=0$ s (before switching on the power supply to the heating rod) from the reconstructed phase at that time instance. Fig. 5.12 shows the spatiotemporal evolution of the phase difference profile. It can be seen that as heat diffuses into the medium, the signature of the defect becomes more pronounced on the phase profile of the probe beam. The thermal stressing brings out the refractive index difference between the defect and the surrounding medium. The defect information is obtained after unwrapping the phase distribution at a time instance. It must be noted that it is not possible to pin point the axial location of the defect. The diffuser converts the object information into speckles to couple information from larger area of the object onto the sensor.

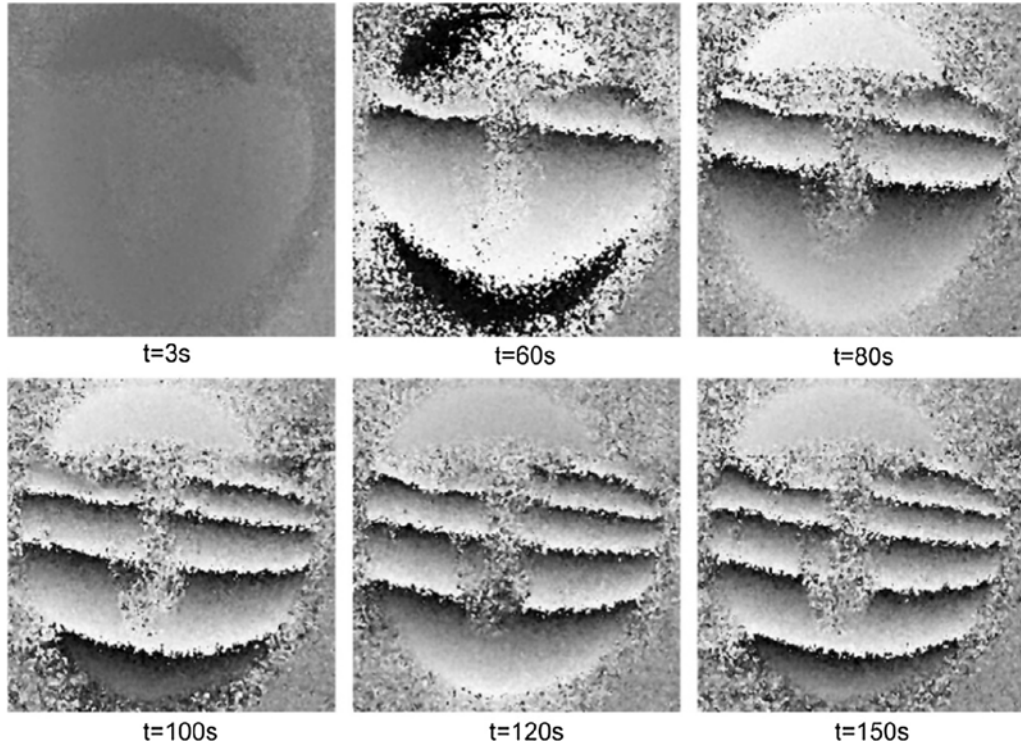


Fig 5. 12: Spatiotemporal evolution of probe beam phase under thermal stressing. This phase distribution is then used for imaging of defects in translucent materials

Fig. 5.13(a) shows the unwrapped phase profile 150 s after switching on the heating source. As the heating source was a point one, it results in a spherical phase on which the object information is overlapped. The spherical phase is nullified by subtracting a digitally inputted phase distribution (Fig. 5.13(b)) from the unwrapped phase distribution isolating the phase distribution due to the defect. The background phase (spherical phase) to be subtracted from the unwrapped phase was determined numerically for every row from the least square fit of the unwrapped phase profile (along the x-direction) with a function of the second-degree polynomial. Second-degree polynomial is chosen since the heat distribution outside of the defect due to a point heating source will lead to a quadratic phase.

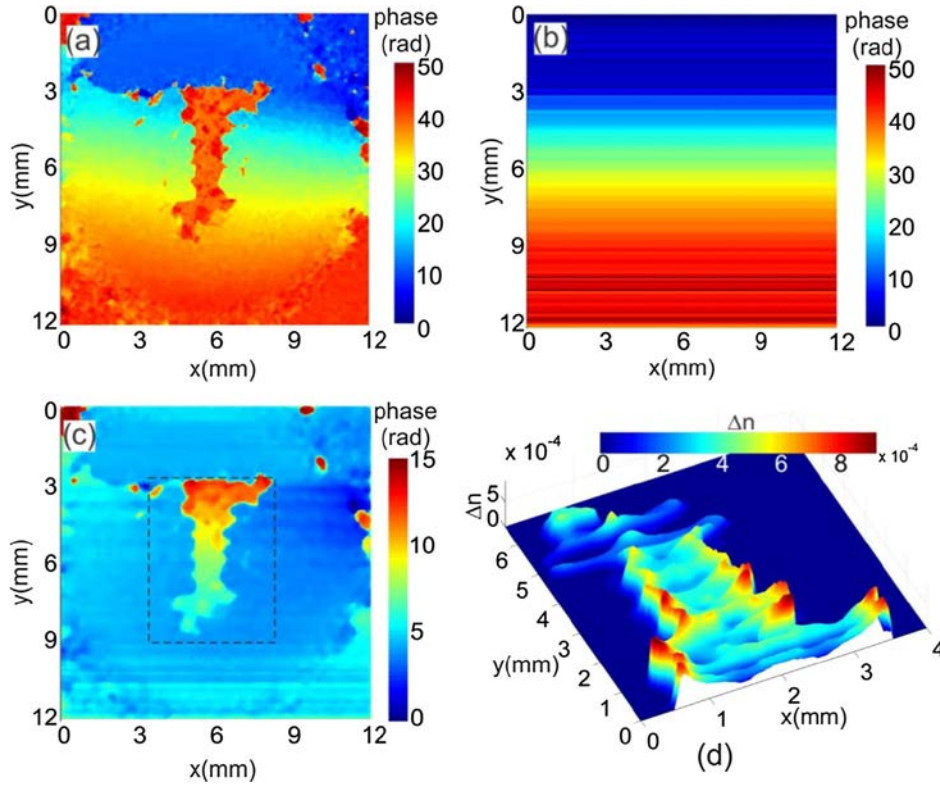


Fig 5. 13: Defect characterization by thermal stressing. (a) Unwrapped phase difference obtained by Goldstein branch cut method for the wrapped phase map at $t=150$ s (Fig. 11). (b) Numerical phase obtained by row wise least square fitting of unwrapped phase shown in (a) (c) Phase distribution due to defect obtained after subtracting the numerical phase obtained by least square fitting from the unwrapped phase. (d) Three-dimensional refractive index distribution of the defect obtained by Abel inversion of object phase shown inside the rectangle in (c).

Fig. 5.13(c) shows the background eliminated object phase. This phase is then used along with Abel inversion to yield the refractive index profile of the object shown in Fig. 5.13(d). Abel inversion can be used for non-axisymmetric distributions also [325] as can be seen from Fig. 5.13(d), where the phase distribution (Fig. 5.13(c)) from which it was obtained is not axisymmetric. It should be noted that the object is placed behind a diffuser resulting in a random phase distribution (from a single hologram) during reconstructions (due to roughness of the diffuser). The shadow of the defect may be visible in the intensity images. To obtain defect quantitative phase information, we stress the object and subtract the phase information obtained at one time instant from another. This leads to the elimination of phase due to the roughness of the diffuser bringing out the object phase information (Fig. 5.13(a)). So stressing of the object is the most important component in the technique.

5.3 Lensless Fourier Transform digital holography for quantitative phase contrast imaging of Red Blood Cells

5.3.1 Introduction

Quantitative phase imaging of micro-objects including cells provides their thickness/height distribution. This can be used to obtain valuable information about the object such as its shape and dynamics [273,292,326–328]. Thickness information can also be used to classify objects for their recognition/identification that can lead to the determination of the state of its health in the case of living cells [261,262]. Quantitative phase microscopy requires direct access to the complex amplitude of the wavefront interacting with the object (object wavefront). This can be achieved by superposing the object wavefront with a known reference wavefront and recording the resulting interference patterns. Digital holographic (DH) microscopy is such an interferometric technique which can provide direct access to the phase of the object wavefront. From the phase information, the thickness profile of the object under investigation can be computed. Off-axis DH microscopy is a single-shot technique to reveal the phase information, and is an ideal tool to investigate the dynamics of micro-objects including cells from a series of recorded holograms/ interferograms [261,262,270,273,283,288–296]. Since a single Fourier transform yields the complex amplitude of the object wavefront at the image plane, this technique provides phase information in almost real-time. A single beam microscopic technique using LFTDH configuration was employed for imaging RBCs. This type of interferometer has been earlier investigated for the measurement of refractive index distributions [296,329]. The numerical evaluation of the digital holograms with and without the object provides the quantitative phase image of the object. The proposed microscope is tested on static and dynamic micro-objects to reconstruct their 3D profiles. The time-dependent thickness variation of RBCs was studied using this technique with nanometer-level temporal stability.

5.3.2 Experimental Realization

The schematic of the proposed microscope is shown in Fig. 5.14. A laser beam is directly allowed to pass through the object. The image is magnified using a microscope objective lens. A diffuser is located at the image plane of the

microscope objective lens, co-located by a pinhole (Inset of Fig. 5.14). The pinhole samples a small portion of the object beam and converts it into a spherical reference beam originating from a point source located at the diffuser plane (image plane of the microscope objective). An imaging sensor is located behind the pinhole. The diffuser allows the coupling of the image to the sensor by converting it to laser speckles (by scattering the light, coming from the image plane in the direction of the sensor). The object beam (beam from the diffuser) and the reference beam (beam from the pinhole) interfere at the sensor plane producing a hologram (interference pattern). Since the pinhole is located at the image plane, this setup generates lens less Fourier transform holograms. The complex amplitude at the reconstruction or image plane using the Fresnel-Kirchoff diffraction integral after applying the Fresnel approximation is given by [182,253] according to Eq. (5.11).

Thus, the numerical reconstruction is fast compared to other reconstruction approaches such as Fresnel transform (which requires multiplication of the Fourier transform with a spherical phase factor), Fresnel transform with convolution, angular spectrum propagation, and phase shifting. In this case, both the real and virtual images are observed simultaneously at the reconstruction plane. By subtracting the reconstructed phase at the diffuser plane with and without the object, quantitative phase images of the object can be obtained. This can then be used to construct the 3D thickness information of the object using the following relationship

$$\Delta\phi(x, y) = 2\pi(n_o - n_r)L(x, y) / \lambda \quad (5.16)$$

where $\Delta\phi$ is the computed phase difference, n_o and n_r are the constant refractive indices of the object and the surrounding medium and L is the object thickness.

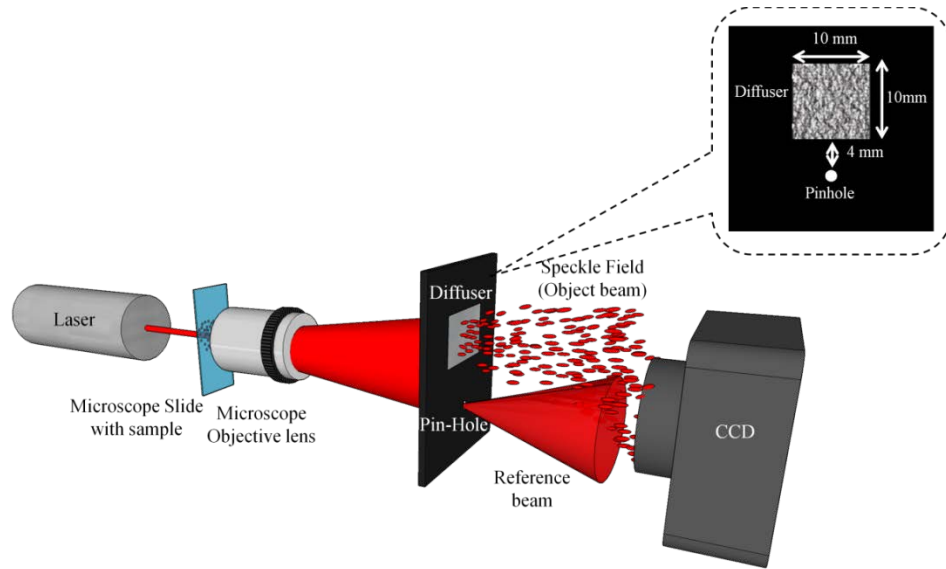


Fig 5. 14: (a) Experimental setup of single beam Lens less Fourier transform DH Microscope, (b) fabrication of wavefront division element. It consists of a ground glass diffuser co-located with a pinhole

Experiments are conducted on static as well as dynamic objects. In the experimental setup, a 120-grit ground glass diffuser (Edmund optics) is located at the image plane of the objective lens, having a window of $10\text{mm} \times 10\text{mm}$ (Inset of Fig. 5.14). It has low transmission loss and for the small angles involved in the present setup, it provides almost uniform illumination at the sensor plane. A pinhole, co-located with the diffuser (used to couple the object information onto the sensor in this off-axis geometry), is fabricated from an unmounted pinhole (Newport) by cutting out a portion of the metal plate containing it, for easy placement closer to the diffuser. The pinhole has a diameter of $40\ \mu\text{m}$ and is placed $4\ \text{mm}$ away from the edge of the diffuser (Fig. 5.14). The size of the pinhole is selected with regards to the fact that it should sample only a very small portion of the object beam so that the generated spherical reference beam is un-modulated by object information. In addition, it should pass enough intensity to produce high contrast interference fringes. The distance of the sensor from the diffuser-pinhole plane (d) and the lateral displacement between the diffuser and pinhole are chosen to satisfy two conditions, (i) the lateral speckle size at the sensor should be greater than twice the sensor pixel size and (ii) the maximum angle subtended between the reference (from pinhole)

and the object beam (from diffuser) must be lower than the angle required by the sampling criteria (the maximum possible resolvable fringe frequency is twice the pixel size).

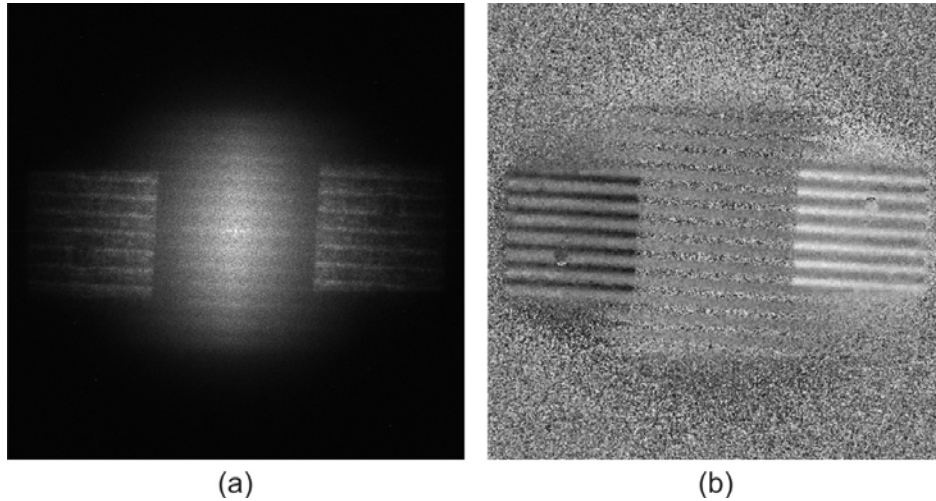


Fig 5. 15: Results obtained for a phase grating. (a) Reconstructed intensity profile at the diffuser plane and (b) Phase contrast image of the grating

In the first set of experiments, a phase grating having 40 lines/*mm* is used as the object. It is illuminated using a commercial grade laser pointer ($\lambda = 532 \text{ nm}$, max output power $< 10 \text{ mW}$) and a 40x microscope objective with $\text{NA} = 0.75$ is used for magnification. An 8-bit CCD sensor with $3.45 \text{ }\mu\text{m}$ pixel pitch and 2000×2000 pixels, kept 23 cm from the diffuser plane, recorded the holograms. Holograms with and without the object are recorded and reconstructed. The phase distribution of the object is obtained after subtracting the phase profile obtained without the object from the phase profile obtained with the object. Figures 5.15(a) and 5.15(b) shows the reconstructed intensity and the phase profile, respectively, at the diffuser plane.

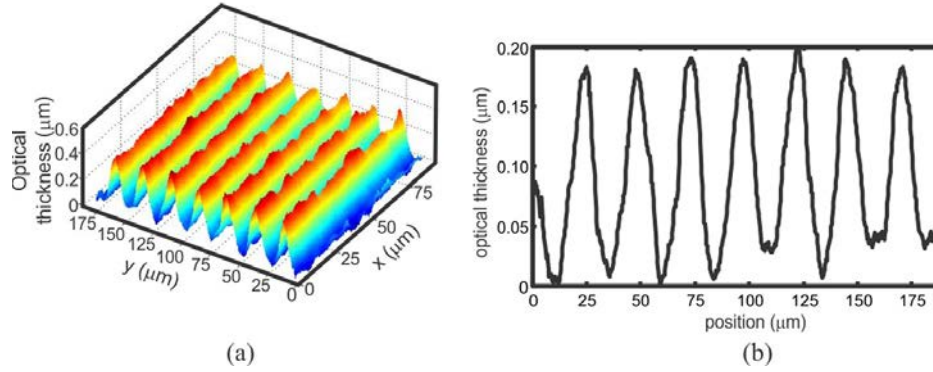


Fig 5. 16: Computed optical thickness distribution of the grating obtained from the phase information. (a) 3D thickness profile and (b) cross-sectional thickness profile

Real and virtual images are simultaneously observable. A low pass filter is applied to the phase distribution to suppress the random phase variation due to speckles. The optical thickness $((n_o - n_r) \times L)$ distribution of the grating is determined using Eq. (5.16) and is shown in Fig. 5.16(a). The cross-sectional thickness profile of the grating is shown in Fig. 5.16(b).

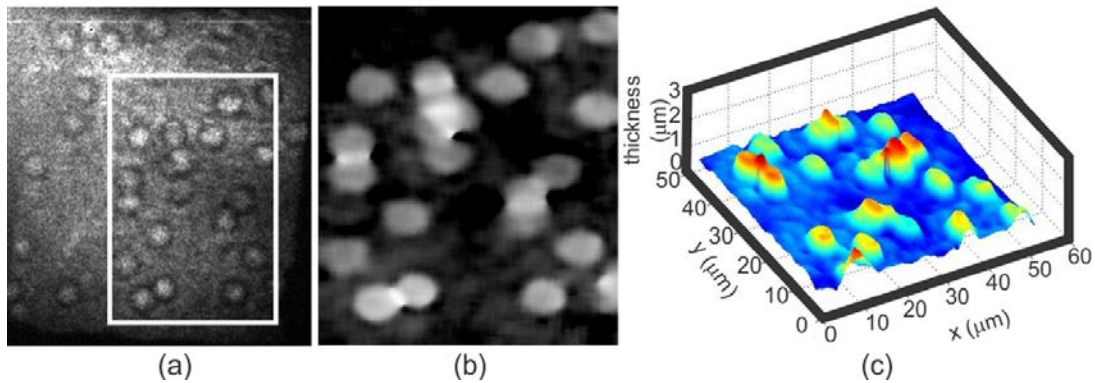


Fig 5. 17: (a) Reconstructed intensity profile of a blood smear at diffuser plane, and (b) the phase contrast image of the rectangle shown in (a). (c) 3D thickness profile computed from the phase-contrast image

In the second set of experiments, RBCs are used as the object. A thin blood smear is made on a glass slide and is covered with a thin cover glass. Here, a diode laser working at 635 nm is used as the light source. An inexpensive commercial grade 40X microscope objective with $\text{NA}=0.65$ is used for the magnification. An 8-bit CCD with $4.65 \text{ }\mu\text{m}$ pixel pitch and 1392×1040 pixels is used for recording holograms and the sensor is kept 20 cm away from the diffuser satisfying the sampling criterion. The holograms are zero-padded to have equal dimensions in ξ

and η directions. This is done to keep the reconstructed pixel sizes in x and y direction the same. Hologram with cells, present in the field of view, is recorded first. The slide is moved such that there is no RBC in the field of view and a second hologram with the object beam passing through the surrounding medium (plasma) is recorded. Figure 5.17(a) shows the reconstructed intensity at the diffuser plane and RBCs can be observed in the field of view. A phase contrast image for this case is shown in Fig. 5.17(b). The thickness of the cells is determined by using a constant refractive index value of 1.40 for the RBC and 1.34 for blood plasma[330]. The 3D thickness distribution is shown in Fig. 5.17(c). For dynamic studies of RBCs, an oil immersion 100X microscope objective with NA=1.25 is used for magnification. The remaining microscope elements stay the same. At first, the stability of the setup is determined from the path length variations when a microscope cover slide is used as the object. For this study, holograms are acquired at the rate of 1Hz for 5 min and the path length changes are computed. The mean of the standard deviation of the path length variation across the object (256×256 pixels) provided the temporal stability of the technique which is found to be 1.24 nm. This is shown in Fig. 5.18, which is the histogram of the path length deviation.

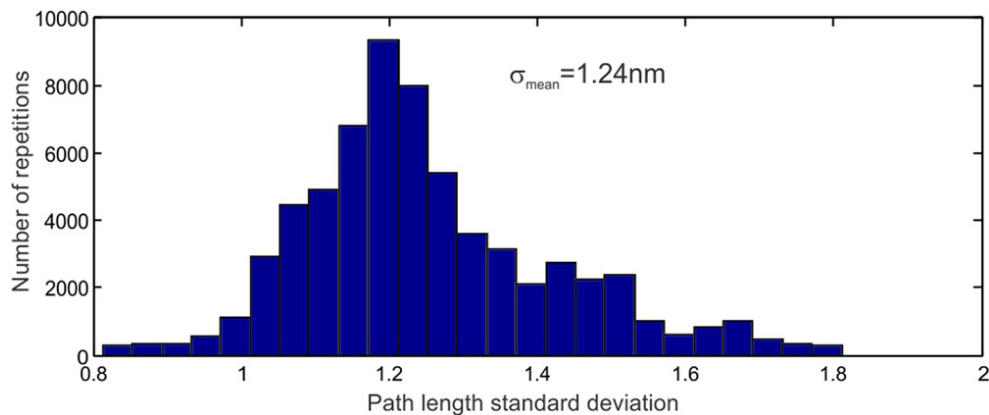


Fig 5. 18: Histogram of the path length fluctuation. The computed mean fluctuation was 1.24 nm

For dynamic imaging of red blood cells, no glass slide is used to cover the thin smear. Holograms are acquired at a rate of 1 Hz and stored on the computer. A single reference hologram with no cells present in the field of view is also recorded.

The time-varying phase contrast images are computed after phase subtraction. The thickness of the cell at each time instance is computed from this phase information. Fig. 5.19(a) shows the observed intensity pattern at the diffuser plane at time $t = 0$ s, for a single cell. Fig. 5.19(b) is the computed phase contrast image for this cell. The three-dimensional thickness profile of this cell is shown in Fig. 5.19(c). The expected doughnut-shape of RBC is observable. Fig. 5.19(d) shows the cross-sectional thickness profile along the line shown in Fig. 5.19(b). From this figure, the doughnut shape of the cell is more evident. The time evolution of cell thickness is obtained from a series of phase profiles computed from sequentially acquired holograms. The measured variation in thickness with time is plotted in Fig. 5.19(e) for the points shown in Fig. 5.19(b). These measured values are comparable with those reported in the literature [291,302].

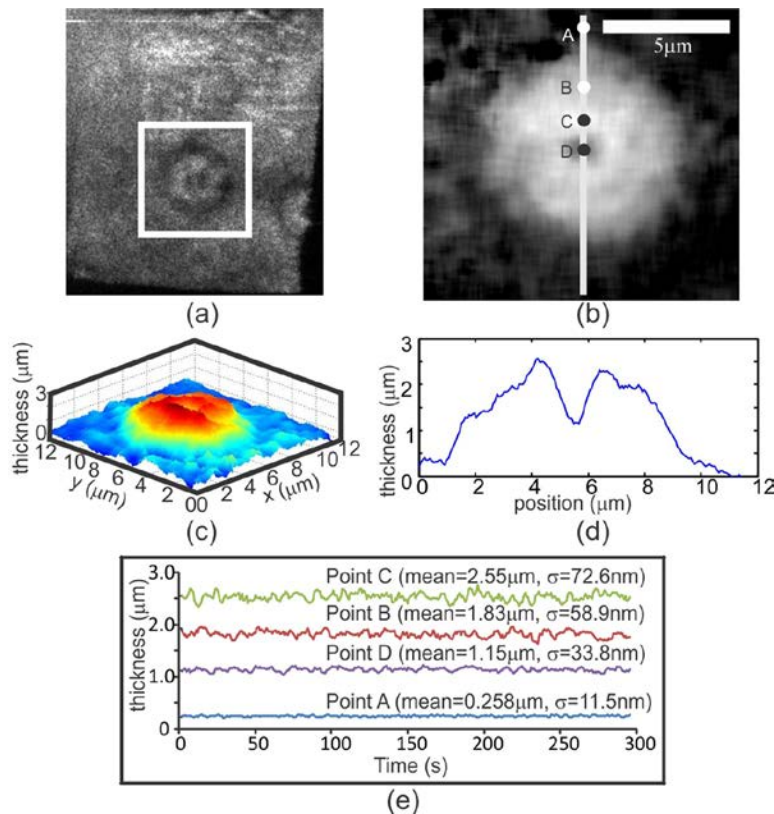


Fig 5. 19: Experimental results obtained for red blood cells using 100 microscopic objective (a) Intensity profile, (b) phase contrast image (c) 3D thickness profile and (d) cross-sectional thickness profile along the line shown in (b). (e) Temporal evolution of cell thickness at points shown in (b), mean and standard deviations of the thickness fluctuations are also given

5.4 Discussion

A single beam Lensless Fourier transform digital holography configuration is employed for (1) mapping refractive index distributions, which can be used to investigate temperature profile of phase objects using lens-less Fourier transform digital holography and using the Abel inversion algorithm for obtaining the local refractive index values for axially symmetric phase distributions (2) quantitative phase contrast imaging of micro-objects such as human erythrocytes (RBCs). Lens-less Fourier transform geometry allows numerical reconstruction using a single

Fourier transform making the fast display of computed phase maps possible. In the case of macroscopic objects, spatio-temporally evolving refractive index profiles are computed from the phase difference measured using phases obtained with and without object information. Heat flow can be imaged and quantified from the refractive index distribution. The technique is also used for defect detection in the case of dielectric mediums using the fact that the heat diffusion across the discontinuity or the defects is different than its surrounding medium and will result in a different phase profile at the defect compared to the continuous medium. Defects in translucent mediums are quantified by thermally stressing the sample and comparing the resulting phase with the phase before the heat source was switched on. Digital holography allows the comparison of the reconstructed phase with a digitally inputted phase and this concept is used to eliminate the phase change due to heat diffusion in the continuous sample to bring out the phase change occurring to the probe beam due to the defect alone. Thus a relatively simple, effective and accurate method of imaging refractive index profile for characterizing phase objects on their ability to conduct heat, which in turn aids in defect detection is developed.

In the case of microscopy, the proposed microscope does not require a separate reference beam, making it rugged with high temporal stability and is suitable for the measurement of dynamic parameters of micro-objects. It can also be used in the case of reflecting objects. Only a single Fourier transformation is required for the reconstructions, making it a very effective tool for quasi-real time 3D profiling of

living cells. The phase subtraction (with and without the object), takes care of the system aberrations providing the liberty to use low-cost optics. Since the object and the reference beams originate from the same wavefront, laser diodes can be used as sources. CMOS sensors (such as webcams) can be employed for recording the holograms, making the construction cost of the microscope very low. The dimensions of the microscope can be further reduced by folding the beam after the diffuser using a mirror, making it compact and field-portable. Work is progressing in the direction of converting the developed technique to a field-portable device along with the necessary software.